Microsystems: Measuring Mixing Efficiency Using Statistical Entropy

Marco Camesasca[1], Miron Kaufman[2], Ica Manas-Zloczower[1]
[1] Dept. of Macromolecular Science, Case Western Reserve University
Cleveland, Ohio, 44106, USA
[2] Physics Department, Cleveland State University
Cleveland, Ohio, 44115, USA

ABSTRACT

Microfluidic systems (lab-on-a-chip devices) are employed in micro-technology having applications in protein and DNA analysis, sensors, and micro electronics mechanical systems. These systems operate in a pressure driven flow regime with no moving parts to drag the fluids. Our research aims at developing rigorous assessment and quantification of mixing in microchannels. The work presented is based on numerical simulations of flow in different geometries coupled with mixing assessment using entropic measures. The results show enhanced mixing efficiency for the geometry similar to the staggered herringbone mixer by comparison with a mixer with straight diagonal ridges and lack of mixing in a non-patterned channel.

1. INTRODUCTION

Micromixers are microfluidic systems where two or more fluids are mixed; these systems are used, for example, for controlling the dispersion of minor components in Poiseuille flows and for homogenization of solutions in chemical reactions.[1] Microfluidic devices generally operate in a laminar flow regime and consequently mixing is a difficult task.[2] Due to the typically low Reynolds number and the high Peclet number encountered in such systems, mixing is primarily achieved by manipulating the channel geometry[3].

Mixing evaluation in microchannels has primarily relied on observing color or intensity variations of a dye as it is transported through the mixer,[4,5] or studying the interface configuration between two fluids, one of which fluorescent, by employing confocal fluorescence microscopy.[6] Numerically, the performance of different mixers was based on studying virtual particles trajectories computed using a Lagrangian method and interpreting the results in terms of computed Poincare maps[7,8] or Lyapunov exponents. In this case, the underlying assumption in the interpretation of the results is that mixing can be achieved efficiently only in chaotic flows.[4,7,8] However, chaos is not a pre-requisite for mixing and therefore a lack of chaos does not implicitly preclude system homogenization.

In the present work we are presenting a couple of alternative ways to characterize and quantify the degree of mixing in microchannels. We propose to use numerical simulations to study the flow patterns in channels with various geometries and to employ the conditional Shannon entropy to rigorously quantify the dynamics of mixing for two miscible fluids distinguished by color.

The proposed entropic analysis can be also carried out for data obtained in experiments, thus making it universally applicable for mixing evaluation. We also characterize the geometric structures developed in flow with multifractal dimensions thus providing a complementary measure of quality of mixing.

2. THEORETICAL BACKGROUND

2.1. Multifractal Dimensions and Renyi Entropies

The Shannon[9] entropy S is the rigorous measure of mixing or lack of information and it has been used in many different scientific areas.[10,11,12,13] It is uniquely determined from reasonable properties (Khinchin axioms[14]), that a measure of the lack of information or mixing must satisfy: (I) it depends on the probability distribution p only; (II) the lowest entropy (S = 0) corresponds to one of the p's being 1 and the rest being zero (i.e., total information, perfect order, complete segregation); (III) the largest value for the entropy is achieved when all p's are equal to each other (i.e., the absence of any information, complete disorder, perfect mixing); and (IV) S is additive over partitions of the outcomes.

$$S = -\sum_{j=1}^{M} p_j \ln p_j \tag{1}$$

If the last Khinchin axiom is relaxed to consider only statistically independent partitions, Rényi[15] found that the information entropy is replaced by a one-variable function:

$$S(\beta) = \frac{1}{1-\beta} \ln\left(\sum_{j=1}^{M} p_j{}^{\beta} \right) \tag{2}$$

In Equations (1) and (2) M is the number of equisized sub-domains (bins) employed to cover the space analyzed. Equation (2) gives the Shannon entropy (Equation 1) in the limit of $\beta \to 1$. If $\beta > 0$ the function defined in Equation (2) is maximized when all p’s are equal to each other. It follows that: $0 < S(\beta) < \ln(M)$. Thus $S(\beta)/\ln(M)$ constitutes an index of homogeneity: it is 1 for total disorder or homogeneity and is small for high order or segregation.

Multifractals are used to model the geometric structure of complex systems such as the backbone of the percolation cluster or the structure generated in diffusion limited aggregation. While fractals are characterized by a single fractal dimension, multifractals are characterized by a one-variable function or spectrum of dimensions $d(\beta)$. By varying the parameter β we get the Hausdorff dimension when $\beta = 0$, the information (Shannon) dimension when $\beta = 1$ and the correlation dimension when $\beta = 2$. These dimensions are obtained by using the Rényi entropy defined in Eq.(2). A graph of $S(\beta)$ versus $\ln(M)$ shows a straight line dependence for $1 << M << N$ (number of particles). The slope of the line is the ratio: $d(\beta)/D$, where D is dimension of embedding space.

$$d(\beta) \approx D \frac{S(\beta)}{\ln(M)} \text{ for } 1 << M << N \tag{3}$$

As a result, the fractal dimension $d(\beta)$ can be obtained by plotting the Rényi entropy versus the logarithm of the number of bins M and fitting the plot with a linear function.

2.2. Shannon Entropy for Multi-component Systems

The Shannon entropy for a multi-component system with C components distributed in a cross-sectional space divided in M smaller equisized sub-domains (bins) is:

$$S = -\sum_{j=1}^{M}\sum_{c=1}^{C} p_{j,c} \ln p_{j,c} \tag{4}$$

where $p_{i,c}$ is the joint probability that a particle is of component c and is located in bin j. The total entropy is additive in the sense that it is equal to the sum of the conditional entropy $S_{location}$(species) and the entropy of spatial distribution S(location):

$$S_{location}(species) = \sum_{j=1}^{M}\left[p_j S_j(species) \right] \tag{5}$$

$$S_j(species) = -\sum_{c=1}^{C}\left[p_{c/j} \ln p_{c/j} \right] \tag{6}$$

$S_{location}$(species) is an average over the M spatial bins, of the entropy of mixing the C species conditional on bin location. In Equations (5) and (6) above p_j is the probability that a particle is in bin j irrespective of species and $p_{c/j}$ is the probability that a particle is of the type c conditional on being in bin j. S(location) is the entropy associated with the spatial distribution of particles irrespective of their species:

$$S(location) = -\sum_{j=1}^{M} p_j \ln p_j \tag{7}$$

In this work we analyze the mixing of two incompressible fluids (C = 2). Since the density at any location does not change in time, the entropy S(location) is also constant at all times during the process. Thus we concentrate on $S_{location}$(species) which measures the local quality of mixing of the two fluids averaged over space. Since $0 \leq S_{location}(species) \leq \ln(C)$, we normalize the species entropy conditional on locations $S_{location}$(species) on ln(C) to get an index of mixing varying between 0 for perfect segregation and 1 for perfect mixing. The number of bins, M, controls the scale of observation.

3. NUMERICAL PROCEDURE

In our studies we employed FIDAP, a commercial CFD-FEM package to solve the 3D steady-state, isothermal flow of a Newtonian fluid in the various geometries. Massless, non-interacting virtual tracers distinguished by color were randomly placed at the entrance of the flow channel and their position was followed along the channel length. We employed a fourth-order Runge-Kutta method in the particle tracking algorithm.

4. SIMULATIONS

We consider three different microsystems: a rectangular channel with no patterns on the walls, a rectangular channel with simple straight ridges on the bottom wall and a rectangular channel with asymmetric V ridges similar to the staggered herringbone mixer (SHM).[3]

The Straight Diagonal Ridge (SDR) geometry has all equal ridges placed at an angle of 35° with respect to the x axis. The Asymmetric V Ridge (AVR) mixer has ridges with two arms asymmetric in length both forming an angle of 35° with the x axis. Every six ridges the geometry is inverted so that each six ridges form the mirror image of the previous six ones. Schematics of these two geometries are shown in Figure 1. To validate our numerical work we also analyze the mixing process in the staggered herringbone mixer (SHM) and compare it to the published experimental results.[3]

The boundary conditions for the CFD simulations of the pressure driven flow are an average velocity in the down channel direction of 1 m/s and no slip at the solid surfaces. The fluid is Newtonian with density of 10^3 kg/m^3 and viscosity of 10^{-3} Pa s. We used 8000 tracers of two colors (4000 per species) randomly placed at the inlet of the mixers to completely fill the cross-section and follow their trajectories to observe the dynamics of the mixing process.

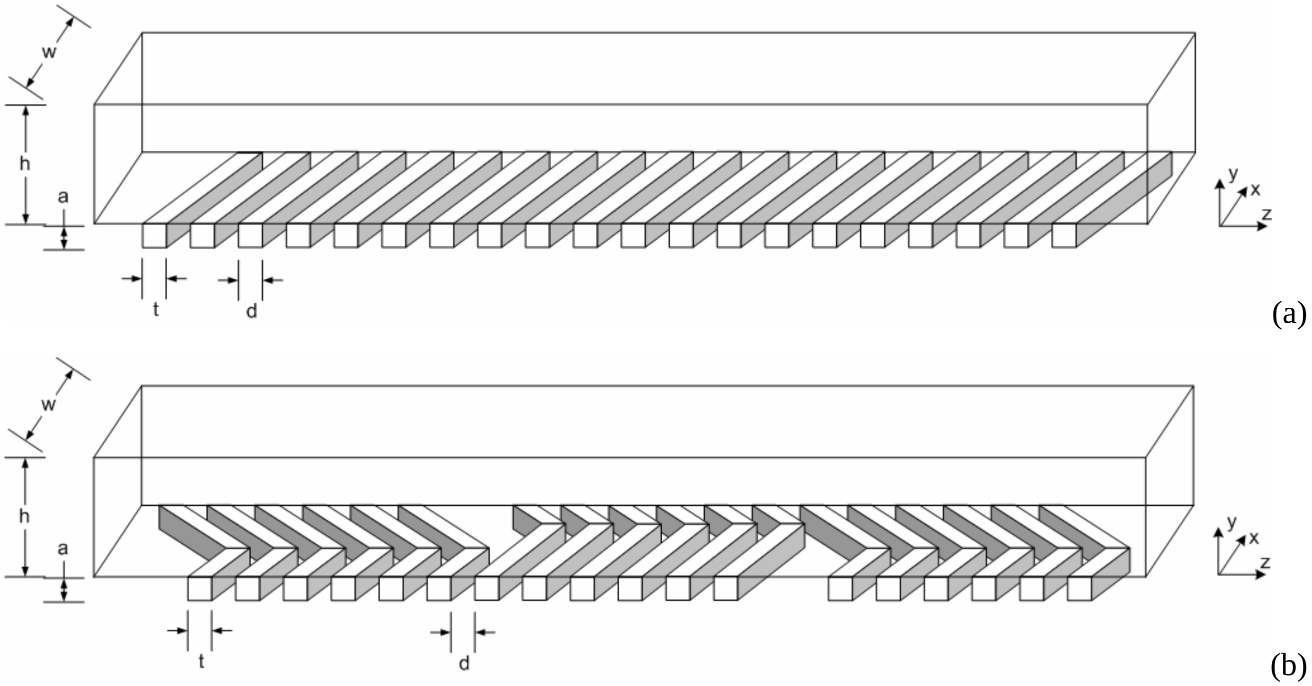

Figure 1. (a) Geometry of the channel with straight diagonal ridges (SDR). The height *h* is $8\cdot10^{-5}$ m, the width *w* is $2\cdot10^{-4}$ m, the ridge thickness *t* and the ridge height *a* are both $2\cdot10^{-5}$ m; the minimum distance between two consecutive ridges *d* is $2\cdot10^{-5}$ m. The angle that each ridge forms with the x axis is 35°. (b) Geometry of the channel with asymmetric V ridges (AVR). The height *h* is $8\cdot10^{-5}$ m, the width *w* is $2\cdot10^{-4}$ m, the ridge thickness *t* and the ridge height *a* are both $2\cdot10^{-5}$ m, the minimum distance between two consecutive ridges *d* is $2\cdot10^{-5}$ m. The angle that each portion of the ridge forms with the x axis is 35°.

The initial tracer distribution and progression of mixing of the two fluids are shown in Figures 2left and 2center for the SDR micromixer and the AVR micromixer, respectively. There is no change between the inlet and exit configurations in the straight channel geometry and we do not present this result graphically. Visual inspection of those images provides a qualitative assessment of mixing in different geometries. And although formation of striations can be clearly observed for both the SDR and the AVR geometries, mixing seems to progress faster in the AVR system by comparison with the SDR geometry. Figure 2right shows the results obtained in the experiments in reference [3], providing a side by side comparison with our results from the CFD calculation.

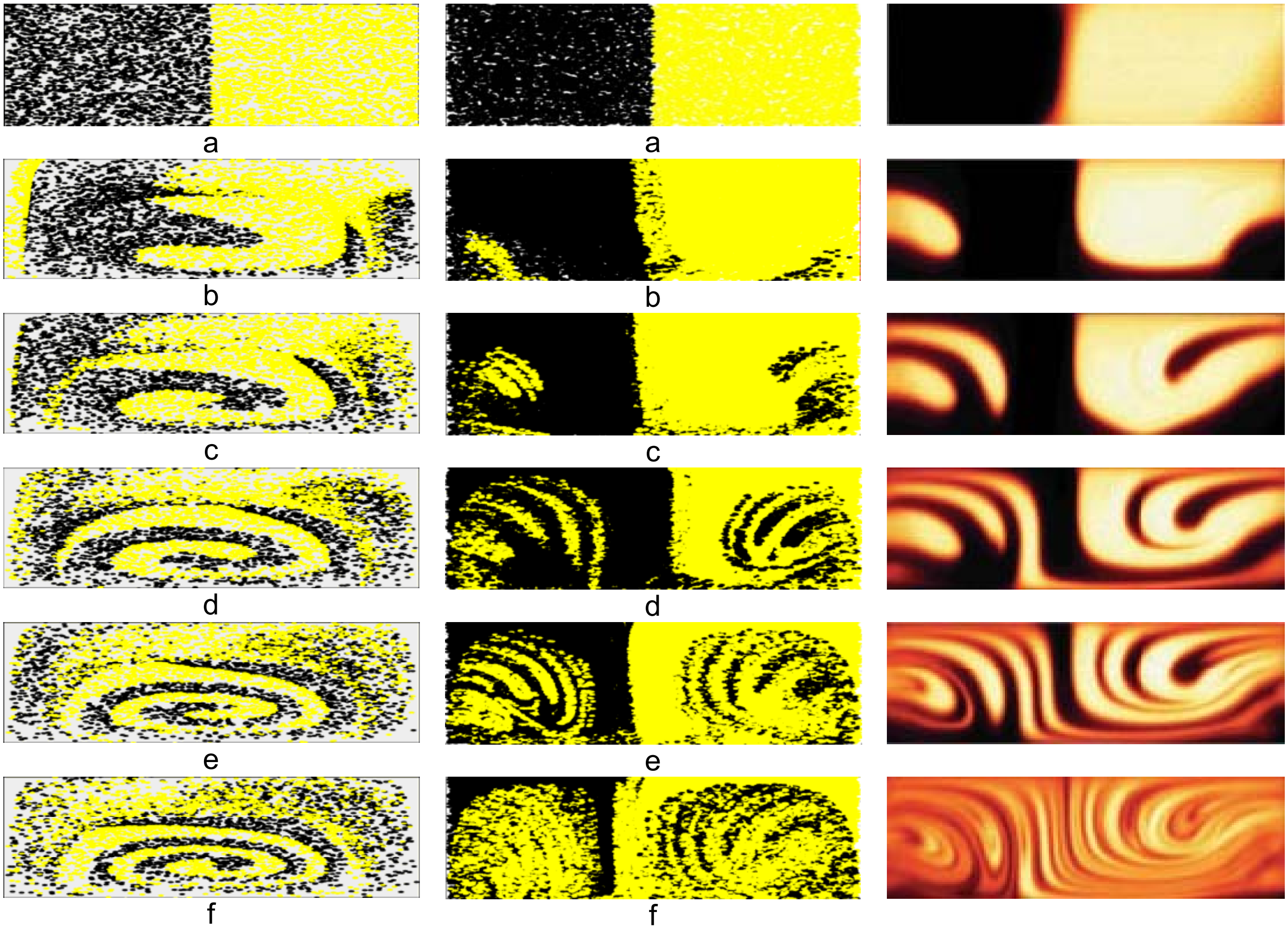

Figure 2. Evolution of mixing in the SDR (left) and AVR (center) micromixer simulations. (a) Initial condition (xy cross section at z=0); all consecutive images represent cross-sections of the system at: (b) z= $1\cdot10^{-2}$ m; (c) z= $2\cdot10^{-2}$ m; (d) z= $3\cdot10^{-2}$ m; (e) z= $4\cdot10^{-2}$ m; (f) z= $5\cdot10^{-2}$ m. Pictures from reference 3 represent the evolution of mixing in the SHM.

5. RESULTS

5.1. Entropic Analysis

There is no mixing between the two species in the straight channel. For the SDR and AVR geometries, the level of mixing at different cross-sections along the channel length are plotted in Figure 3 in terms of the normalized $S_{location}$(species). One can clearly observe that the normalized $S_{location}$(species) attains higher values in the AVR channel by comparison with the SDR geometry. Concerning the dynamics of the mixing process, one can distinguish a higher initial slope of the normalized $S_{location}$(species) versus channel length in the case of the AVR configuration by comparison with the SDR mixer.

To facilitate comparison of the three systems, in Figure 4 we plot the normalized $S_{location}$(species) versus the distance from the inlet for the three different geometries at 1500 bins, the highest level of resolution/smallest scale of observation used in the analysis. The AVR mixer clearly shows the highest mixing efficiency both in terms of mixing quality and mixing rate.

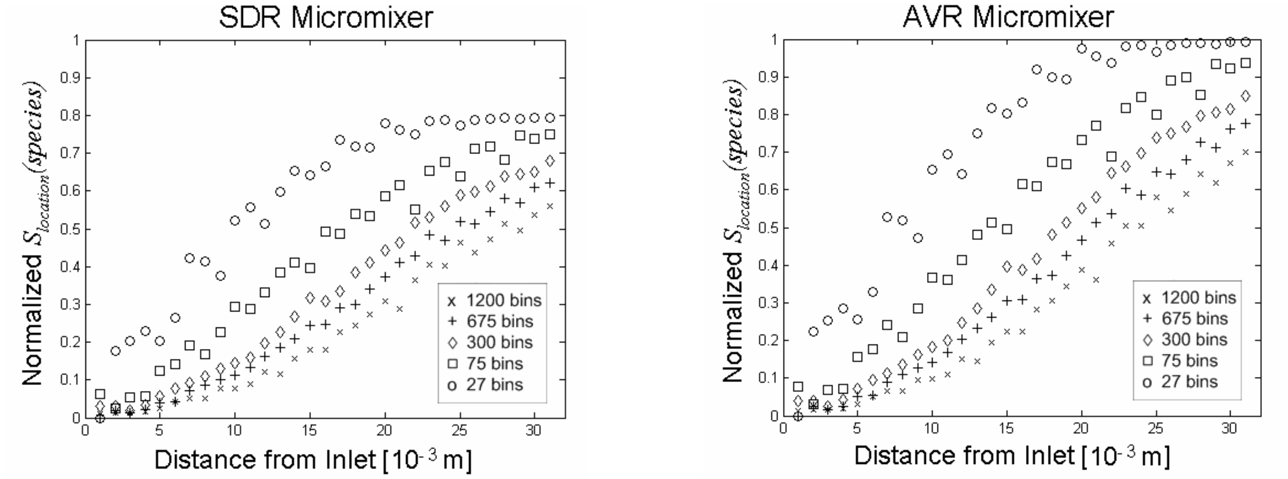

Figure 3. Normalized *$S_{location}$(species)* versus distance from the inlet for different number of bins. The maximum values reached by the AVR mixer are higher by comparison with the SDR mixer. The effect of the number of bins used in the analysis is clearly visible.

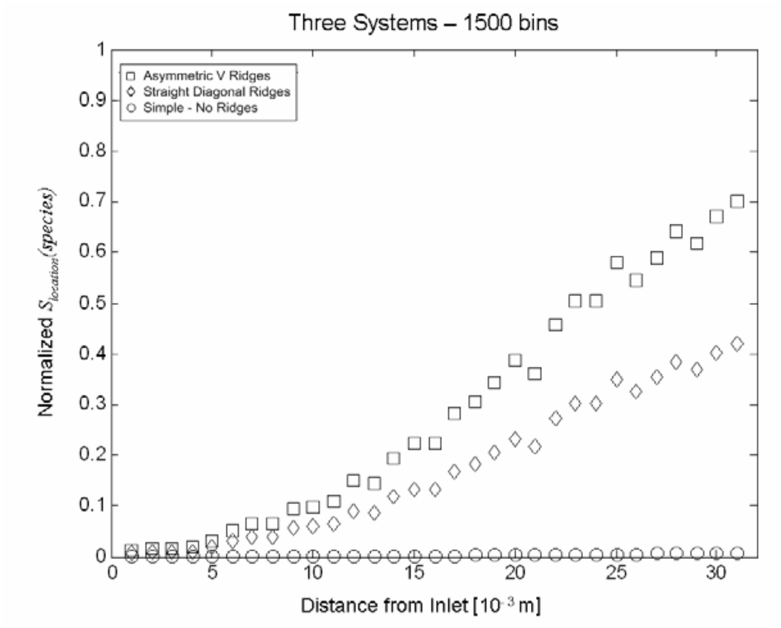

Figure 4. Comparison of mixing efficiency in the three different geometries.

We finally apply our entropic analysis on the experimental results obtained by Stroock et al.[3] To compute the entropy, each of the six cross sections in Figure 2center has been converted to gray scale, divided into 1500 bins and $S_{location}$(species) was computed from Equations (5) and (6). The results are presented in Figure 5 along with the results obtained in the numerical simulations for the AVR mixer. The result of the entropic analysis is rewarding as it demonstrates that the methodology proposed here can be successfully applied to both numerical simulations and experiments.

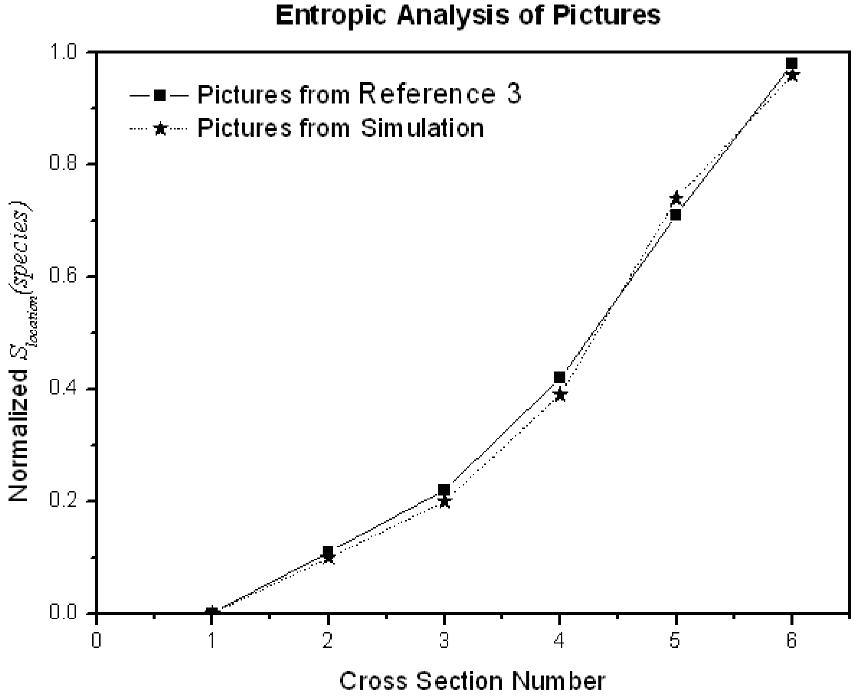

Figure 5. Comparison of the entropic analyses of the pictures presented in figure 2center and right. Every picture is divided into 1500 bins and the entropy $S_{location}(species)$ is calculated based on the probabilities $p_{1/j}$ and $p_{2/j}$ representing the averages over the total number of pixels in bin *j* for the black and white levels respectively.

5.2. Fractal Analysis

We analyze the structures generated in the staggered herringbone mixer and reported by Stroock et al.[3] in terms of their fractal dimensions. The six images shown in Figure 2right were converted to grayscale. Each pixel j has a gray scale value x_j varying between 0, black, and 255, white. Renyi entropies were calculated for each image by using the probability p_j, computed using the reading from each pixel

$$p_{j} = \frac{x_{j}}{\sum_{j} x_{j}} \tag{8}$$

To determine the multifractal dimensions we analyzed the pictures at different scales. To this end we form equal sized bins, each containing several pixels. The *x* value associated with a bin is the mean of the *x* values from the pixels belonging to the bin. The probability associated with the bin is obtained from Equation (8) and then used to compute the Rényi entropy, Equation (2).

The slope of the plot of the Renyi entropy $S(\beta)$ versus $\ln(M)$ for $M >> 1$ is $d(\beta)/D$, with $D = 2$. For each picture we considered 10 scales of observation starting from 16058 (number of pixels). The dependence of the multifractal dimension on section and β is shown in Figure 6. The starting section has a dimension 2, since the rectangular section is half filled with one fluid and half with the other fluid. The last section also shows a dimension close to 2, corresponding to a homogeneous configuration. The dimensions are less than two for the intermediate sections, 2 through 5, in view of the less than perfect homogeneity exhibited.

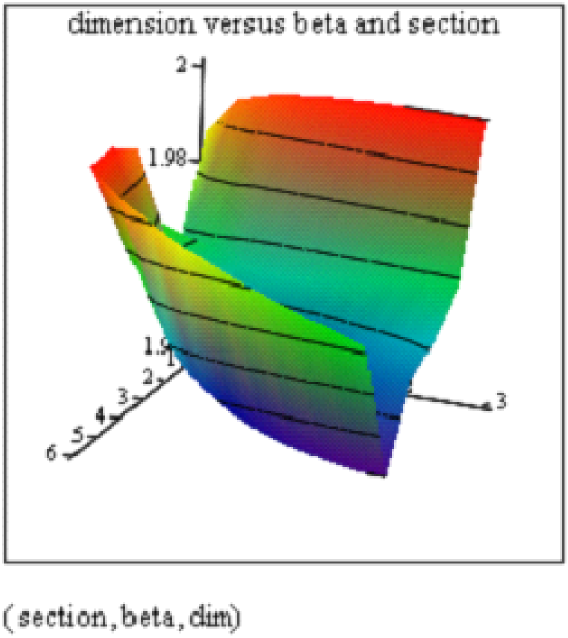

Figure 6. Multifractal dimension vs. section and beta

6. CONCLUSIONS

Microfluidic devices were analyzed for their mixing efficiency using an entropic method. Our results show an enhanced mixing efficiency for the AVR system (a similar version of the SHM mixer) by comparison with the SDR system. We have also analyzed directly the experimental data from the SHM mixer[3] demonstrating the adaptability of this method to both simulations and experiments.

ACKNOWLEDGMENT

The authors thank the National Science Foundation for the financial support this research through grant DMI-0140412.

REFERENCES

1. Jones S.W., Young W.R.: 1994 J. Fluid Mech. 280 149
2. Pfahler J., Harley J., Bau H., Zemel J.: 1990 Sens. Actuat. A 23 431–434
3. Stroock A.D., Dertinger S.K.W., Ajdari A., Mezic I., Stone H.A., Whitesides G.M.: 2002 Science 295 647–651
4. Liu R.H., Stremler M.A., Sharp K.V., Olsen M.G., Santiago J.G., Adrian R.J., Aref H., Beebe D.J.: 2000 J. Microelectromechanical Systems 2 190-197
5. Therriault D., White S.R., Lewis J.A.: 2003 Nature Materials 2 265–271
6. Yamaguchi Y., Takagi F., Watari T., Yamashita K., Nakamura H., Shimizu H., Maeda H.: 2004 Chem. Eng. J. 101 367-372
7. Wang H., Iovenitti P., Harvey E., Masood S.: 2003 J. Micromechanics and Microengineering 13 801-808
8. Niu X., Lee Y.: 2003 J. Micromechanics and Microengineering 13 454-462
9. Shannon C.E.: 1948 The Bell System Technical J. 27 379-423 and 623-656
10. Brooks D.R.: 1998 Evolution as Entropy (Chicago: University of Chicago Press)
11. Allen P.A., Kaufman M., Smith A.F., Propper R.E.: 1998 Psychology and Aging 13 501-518
12. Georgescu-Roegen N.: 1971 The Entropy Law and the Economic Process (Cambridge, MA: Harvard University Press)
13. D’Allessandro D., Dahleh M., Mezic I.: 1999 IEEE Transactions on Automatic Control 44 1852
14. Khinchin A.I.: 1957 Mathematical Foundations of Information Theory (New York: Dover)
15. Rényi A.: 1955 Acta Mathematica Hungarica 6 285-335.